The Accuracy of Preliminary WindSat Vector Wind Measurements: Comparisons With NDBC Buoys and QuikSCAT

Michael H. Freilich and Barry A. Vanhoff

***Abstract*—Two preliminary, six-month long global WindSat vector wind datasets are validated using buoys and QuikSCAT measurements. Buoy comparisons yield speed and direction root mean square accuracies of 1.4 m/s and 25° for the "NESDIS0" product and 1.3 m/s and 23° for the more recently produced "B1" product from the Naval Research Laboratory. WindSat along- and across-wind random component errors of 0.7–1.0 and 2.6–2.8 m/s (respectively) are larger than those calculated for QuikSCAT in the same period. Global WindSat–QuikSCAT comparisons generally confirmed the buoy analyses. While simple rain flags based directly on WindSat brightness temperature measurements alone are shown to overflag for rain systematically, the advanced "Environmental Data Record" rain flag in the B1 product matches well with Special Sensor Microwave/Imager rain detection frequency and preserves the accuracy of the unflagged vector wind measurements.**

***Index Terms*—Ocean surface winds, QuikSCAT, remote sensing, WindSat.**

I. Introduction

WINDSAT was launched in 2003 to demonstrate the capability of polarimetric, microwave radiometers to measure near-surface ocean wind speed and direction in all-weather conditions [1]. Accurate vector wind measurements from WindSat can augment satellite-borne microwave scatterometer data, which since 1991 have increasingly been used to provide all-weather measurements of near-surface wind velocity over the global oceans for research and operational applications [2]. While scatterometers measure the single-frequency backscatter cross section of the ocean surface from a variety of viewing geometries [3], polarimetric radiometers make simultaneous measurements of the brightness temperature ("T_b") of the ocean–atmosphere system from a single viewing geometry, but at a number of frequencies and polarizations.

Spaceborne microwave wind estimation relies upon empirical model functions relating T_b (or, for scatterometers, the normalized radar cross section "σ_o") to the near-surface wind speed and direction. Since the model function and the retrieval algorithms are empirically based, the satellite wind measurement accuracy must be quantified over a wide range of atmospheric conditions. This paper validates WindSat vector wind estimates by comparing them with observations both from operational U.S. National Data Buoy Center (NDBC) meteorological buoys and from the wide-swath QuikSCAT scatterometer.

Buoy measurements have historically been considered the primary comparison data for satellite wind validation (see [4]–[8] and many others), notwithstanding issues of buoy quality control, representativeness (the buoys measure temporal averages at a point, while the spaceborne data are nearly instantaneous spatial averages [9]), buoy inaccuracies in high wind and wave conditions [10], and the need to account for differences due to collocation mismatches in coastal regions dominated by orographic wind modifications. The comparison buoys in this study were selected, based on the number and spatial distributions of the satellite collocations, to be representative of the ocean winds measured by WindSat.

In addition to the NDBC buoy measurements, a well-validated global vector wind dataset was available from the QuikSCAT scatterometer covering the six-month (September 1, 2003–February 28, 2004) period of the WindSat vector wind products. While WindSat–QuikSCAT comparisons were complicated by small systematic cross-swath variations in the accuracy of the QuikSCAT data [11], the global coverage of the satellite–satellite collocations and the fact that both measurements are instantaneous spatial averages allowed for construction of a larger, and more direct, set of comparisons than was possible with buoys.

Comparisons are analyzed here in the context of the random component error model of Freilich *et al.* [6], [7]. For both the NDBC and QuikSCAT comparisons, the error model was extended to accommodate different error magnitudes in the along-wind and cross-wind components [11], and the analysis accounts for errors in both the satellite data being validated and the comparison measurements (buoy or QuikSCAT).

This paper is organized as follows. The WindSat, QuikSCAT, and NDBC buoy datasets are briefly summarized in Section II. Collocation and editing criteria, including the analyses used to select buoys representative of the satellite measurements, are described in Section III. Section IV presents accuracy estimates based on the buoy and QuikSCAT collocations for the highest-quality, nonraining "NESDIS0" WindSat vector wind measurements [12], [13]. A significant fraction of all WindSat measurements were flagged during geophysical retrieval processing as being contaminated by rain. In Section V, comparisons with Special Sensor Microwave/Imager (SSM/I) measurements in the vicinity of the NDBC buoys are used to assess the frequency with which NESDIS0 measurements

Manuscript received February 4, 2005; revised March 8, 2005. This work was supported by the National Aeronautics and Space Administration under Grant NAS5-32965 to Oregon State University.

The authors are with the College of Oceanic and Atmospheric Sciences, Oregon State University, Corvallis, OR 97331-5503 USA (e-mail: mhf@coas.oregonstate.edu).

Digital Object Identifier 10.1109/TGRS.2006.869928

were rain flagged; buoy collocations with rain-flagged WindSat data are then analyzed to characterize the accuracy of the flagged data. At the start of 2005, a second WindSat vector wind dataset (denoted "B1") was produced by the WindSat project. This global dataset was based on refined instrument (T_b) calibrations and used a different model function and different retrieval algorithms than were used to produce the NESDIS0 dataset analyzed in previous sections. In Section VI, we present preliminary characterizations of this new dataset in order to demonstrate the improvements that can be expected from further instrument calibration and processing refinements. Conclusions are summarized in Section VII.

II. Datasets

A. WindSat

The WindSat microwave radiometer on the Coriolis mission (hereafter "WindSat") is the first spaceborne polarimetric radiometer. The mission's primary objective is to demonstrate the ability to measure near-surface wind speed and direction under nearly all-weather conditions using collocated, multifrequency polarimetric microwave radiometer measurements. Details of the WindSat instrument design, ground processing, and preliminary T_b calibration are given in [1], and only a brief review is provided here.

The Coriolis spacecraft flies in a sun-synchronous circular orbit (830-km altitude, 98.7° inclination) with a local ascending node time of $\sim$1800. In this orbit, the antenna spins at $\sim$31.6 revolutions per minute, and the effective swath width (for foreward looks) is $\sim$950 km centered on the satellite subtrack. Although the antenna has a 350 km-wide, aft-looking clear field of view for all but the 6.8-GHz measurements, no aft-looking data were used to retrieve the vector wind estimates examined in the present study.

The WindSat radiometer provides accurate measurements of the brightness temperature of the ocean/atmosphere system for vertical, horizontal, $\pm 45°$, and both left- and right-hand circular polarizations at frequencies centered on 10.7, 18.7, and 37.0 GHz; additionally, vertically and horizontally polarized brightness temperature data are obtained at 6.8 and 23.8 GHz. Brightness temperature differences between the $+45°$ and $-45°$ channels are used to calculate the third Stokes parameter, and differences between left- and right-hand polarized channels yield the value of the fourth Stokes parameter. The Earth incidence angle of the measurements varies from 50° to 55°, depending on frequency. Since the instrument uses a single 1.8-m reflector, the spatial resolutions of instantaneous fields of view vary from 40 $\times$ 60 km at 6.8 GHz to 8 $\times$ 13 km at 37 GHz. To construct both the NESDIS0 and B1 datasets analyzed here, the WindSat ground processing system projected all T_b measurements onto the grid defined by the 6.8-GHz measurements. All T_b data were then interpolated to a 12.5-km grid (defined approximately by every fourth 37-GHz measurement in the along-scan direction and every 37-GHz T_b measurement in the along-track direction [14]), and geophysical retrievals were obtained at each grid location. Thus, while the true resolution of the WindSat vector winds is no better than 50 km (the resolution of the 6.8-GHz T_b measurements), the environmental data records contain vector wind estimates every 12.5 km and are oversampled by at least a factor of four in each spatial dimension.

Changes in atmospheric water vapor and liquid water, small-scale ocean surface roughness and foam (influenced primarily by winds), sea-surface temperature variations, and the presence of rain all cause variations in the WindSat T_b measurements. As different geophysical processes influence T_b differently as a function of frequency and polarization, WindSat's multiple, simultaneous, collocated measurements covering a range of frequencies and polarizations can in principle be used to estimate simultaneously the full suite of geophysical quantities [12], [13], [15]–[17].

Several different WindSat vector wind datasets have been produced, based on different T_b calibrations, different empirical model functions, and different wind retrieval and ambiguity removal algorithms. In this paper, we examine two preliminary WindSat datasets to estimate the impacts that improved calibrations and algorithms might have on the final vector wind products.

1) NESDIS0 Dataset: The initial six-month, global WindSat vector wind dataset ("NESDIS0") was produced by Jelenak *et al.* [12], [13] and released in late July 2004 [14]. It was based on the version 1.5.1 Science Data Records (SDRs), the first comprehensively calibrated WindSat T_b dataset. During model function and algorithm development for NESDIS0, the version 1.5.1 SDR data were found to have constant and swath-dependent biases. To the extent possible, corrections to these T_b calibration errors were incorporated into the NESDIS0 model function and retrieval algorithms.

A multiple-step approach was used to calculate the NESDIS0 vector winds [14], [18]. Weighted sums of horizontal and vertical polarization brightness temperature measurements at selected frequencies, combined with an empirical radiative transfer model, were first used to retrieve integrated water vapor, cloud liquid water, sea-surface temperature, and wind speed separately at each measurement location. Sensitivity to wind direction is largest for the polarimetric measurements, so wind direction was then estimated by minimizing the weighted sum-square differences between an empirically determined model function and the third and fourth Stokes parameter measurements at 10.7, 18.7, and 37 GHz, using the retrieved SST, cloud liquid water, integrated water vapor, and wind speed retrievals as parameters.

As with scatterometers, the empirical radiometer model function has directional symmetries, resulting in local objective function minima at multiple directions for each retrieval. In contrast with scatterometer retrievals in which the objective function is minimized with respect to both wind speed and wind direction (and thus wind speeds can vary slightly between ambiguities), the serial NESDIS0 algorithm resulted in a constant wind speed for all ambiguities in a given retrieval. A median filter approach, based on initialization of the ambiguous directions using the operational NCEP 10-m wind direction at each WindSat measurement location, was employed to select a unique wind direction [12], [14], [18].

Several Environmental Data Record (EDR) quality flag bits are provided for each vector wind solution [14]. Only NESDIS0 retrievals for which EDR quality flag bits 4–27 and bit 29 were not set were considered "valid" and analyzed in this study. Rain-free vector wind measurements did not have EDR quality flag bit 2 set, while potentially rain-contaminated measurements (discussed in more detail in Section VI) had the bit set. EDR quality flag bits 3 ("Wind Speed"), 28 ("Warm Load Anomaly"), and 30 ("RFI Area") were not considered in our analyses.

2) B1 Dataset: A second six-month global vector wind dataset, produced by Bettenhausen *et al.* at the Naval Research Laboratory, was made available in January 2005 and is here denoted "B1." These wind estimates were based on version 1.6.1 SDR T_b data, which have improved calibration accuracies and better Earth locations than did the 1.5.1 SDRs. Details of the empirical model function and retrieval algorithms are presented in [17]. Of importance to this study, the B1 physically based two-stage retrieval approach yielded four ambiguities (separated by $\sim 90°$) for virtually every valid wind retrieval, in contrast to the NESDIS0 dataset which had many solutions with fewer ambiguities [13]. The B1 retrieval solved simultaneously for wind direction as well as wind speed, sea-surface temperature, integrated water vapor, and integrated atmospheric liquid water, and thus different ambiguities often had different (although similar) wind speeds.

The quality flags associated with each B1 vector wind solution differed from those provided in the NESDIS0 dataset. All B1 solutions flagged for ice (EDR quality flag bit 6), land (bit 7), inland lakes (bit 9), unusual sea-surface salinity (bit 10), the presence of RFI in 10-GHz T_b measurements (bit 12) or sun glint (bit 13) were discarded and not analyzed further. As discussed in Section VI, a two-bit rain flag was provided for each valid B1 wind retrieval.

B. QuikSCAT

The NASA QuikSCAT mission was launched in June 1999 carrying the first conically scanning, dual pencil-beam SeaWinds scatterometer. Operating at 13.4 GHz, the SeaWinds instrument on QuikSCAT acquires vertically and horizontally polarized σ_o measurements with approximately 25-km resolution over 1800-km and 1400-km-wide swaths, respectively. (The scatterometer dataset used in the present study is here referred to as "QuikSCAT" in order to differentiate it from the measurements acquired by a nearly identical SeaWinds instrument which flew on the ill-fated ADEOS-II/Midori-II mission from December 2002 to October 2003.)

Near-surface wind measurements from the QuikSCAT standard science product [19] were used in this study. Potentially rain-contaminated QuikSCAT measurements were identified based on the tabular, multidimensional histogram-based "MUDH" rain flag [20], [21]; only rain-free QuikSCAT wind retrievals were compared with WindSat or buoy measurements.

Previous QuikSCAT validation analyses, including several based on buoy comparisons similar to those reported here, indicated that these standard, rain-free QuikSCAT vector wind measurements have speed and directional root mean square (rms) accuracies of $\sim$1.2 m/s and 19° respectively for wind speeds from 3–20 m/s, and along-wind and cross-wind random component errors of 0.75 and 1.5 m/s, respectively [11] (see also [22] and [23]). The QuikSCAT measurement geometry and azimuthal diversity varies systematically across the swath, leading to swath-dependent variations in the accuracy of the QuikSCAT wind velocity estimates [11], [23]. Compared with the "sweet zones" (between 250 and 700 km from nadir), QuikSCAT wind measurements in the nadir zone (within $\sim$125 km of the subsatellite track) have slightly greater random speed errors. Nadir random directional errors are likewise $\sim 5°$ larger than in the sweet zones. The lack of horizontally polarized measurements and the small azimuthal diversity in the far outer swath (more than 850 km from the satellite subtrack) lead to large speed errors. Therefore, only QuikSCAT measurements from a 1700-km-wide swath were used in this study.

C. NDBC Buoys

During the six-month period for which WindSat vector data are available, the U.S. National Data Buoy Center (NDBC) had some 60 moored meteorological buoys deployed off North American shores including Hawaii. NDBC data and documentation can be obtained at http://seaboard.ndbc.noaa.gov. Each buoy carried redundant, mast-mounted propeller-vane anemometer systems for measuring wind speed and direction, along with instruments to measure air and sea-surface temperatures, surface atmospheric pressure, and in some cases humidity. The buoys reported anemometer measurements corresponding to 8-min time averages collected hourly. Quality control procedures routinely applied by NDBC and estimates of buoy wind velocity accuracy are given in [24] and [25]. Compared with a variety of satellite and numerical model data, total buoy errors are estimated to contribute random component errors of $\sim$1–2 m/s [9], [11]. In this study, a value of 1 m/s was used for buoy component errors in both the along-wind and the cross-wind directions.

The satellite model functions are tuned to provide 10-m neutral stability wind estimates (i.e., the satellite wind speed is that which would be measured by a perfect anemometer at 10-m height if the atmosphere is neutrally stratified). Prior to comparison with satellite measurements, the buoy measurements of temperature, pressure, and humidity were used to transform the raw anemometer-height wind speeds to 10-m equivalent neutral stability speeds using the approach of Liu and Tang [26] as in [7]. Buoy measurements for which both air and sea-surface temperature measurements were not available were discarded, as were data from buoys having anemometer heights less than 5 m [7].

III. Collocation and Editing

Spatial and temporal variations in the true wind field can result in differences between even perfect satellite and buoy measurements. The fundamental incompatibility between the satellite's instantaneous spatial average and the buoy's point temporal average can lead to differences even when both observations are obtained at the same time and the buoy is located at the center of the satellite measurement. Mismatches in the times and locations of the comparison measurements cause differences since the wind field itself may vary with space and time. Many of the NDBC buoys are located in coastal regions where local topography creates small-scale wind features having large

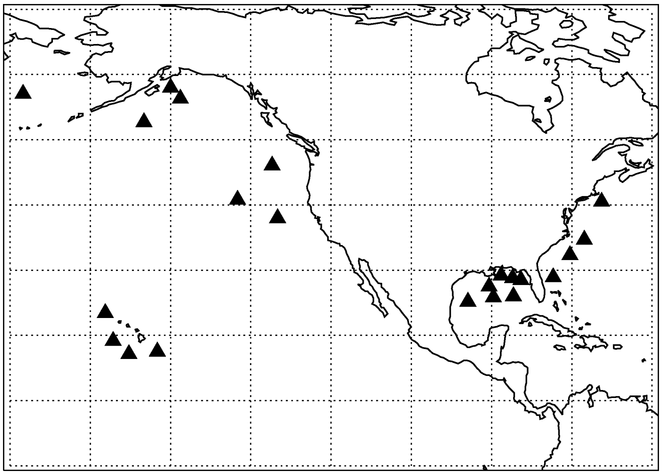

Fig. 1. Locations of the 22 selected NDBC buoys.

TABLE I
NDBC OCEAN BUOYS SELECTED FOR ANALYSIS. "NPTS" IS THE TOTAL NUMBER OF NONRAINING WINDSAT COLLOCATIONS. CENTROID DISTANCE IS DENOTED BY "Δ," AND VECTOR CORRELATION BY "ρ"

Buoy #	Lat (°N)	Lon (°E)	npts	Δ (km)	ρ
41001	34.68	287.34	5262	0.3	1.72
41002	32.31	284.65	5290	1.0	1.68
41010	28.92	281.53	5426	0.6	1.63
42001	25.84	270.34	5111	0.4	1.58
42002	25.17	265.58	5165	0.4	1.24
42003	26.01	274.09	5204	0.2	1.54
42036	28.51	275.49	5429	0.3	1.40
42039	28.80	273.94	5077	3.9	1.52
42040	29.18	271.79	3813	9.0	1.53
42041	27.50	269.54	5532	0.3	1.62
44008	40.50	290.57	3592	10.6	1.56
46001	56.30	211.83	5580	0.7	1.71
46005	46.05	228.98	6855	0.8	1.68
46006	40.80	222.52	6011	0.3	1.61
46035	57.05	182.42	8060	0.1	1.71
46059	37.98	230.00	6581	0.5	1.62
46066	52.70	205.02	5804	0.9	1.58
46080	58.00	210.00	5028	1.3	1.64
51001	23.43	197.79	5517	0.1	1.64
51002	17.14	202.21	5145	0.8	1.05
51003	19.16	199.26	3857	0.5	1.22
51004	17.52	207.52	5124	0.5	1.24

spatial gradients in speed and direction (see [27]–[29] and many others). "Collocated" satellite measurements are usually located systematically seaward of near-coastal buoys, where orographic influences on the surface wind are typically smaller than at the buoy location. If differences between satellite and buoy measurements are to be interpreted as errors in the satellite data, it is essential to use buoys located in areas where the buoy wind measurement is representative of the wind at the nearby locations sampled by the satellite.

Representative buoys were selected using objective collocation criteria that did not depend on comparisons between satellite and buoy wind measurements. Based on previous studies [4], [7], the maximum temporal and spatial differences between buoy and satellite observations were restricted to 30 min and 50 km, respectively. Since WindSat observations are reported on 12.5-km centers, multiple WindSat measurements were typically collocated with a single buoy observation. For each buoy, the centroid of all WindSat measurements within the collocation thresholds over the six-month dataset was calculated. The distance between the centroid and the buoy location was small for open-ocean buoys that were essentially surrounded by WindSat observations over the course of the six months. For 35 of the 60 ocean buoys, the presence of land precluded wind retrieval from large regions landward of near-coastal buoys, leading to centroid distances greater than 12.5 km from the buoy location; these buoys were deemed unrepresentative and excluded from subsequent analyses. Of the 25 buoys having centroid distances less than 12.5 km, two were eliminated from further analyses since they had fewer than 330 collocations each (compared with a mean of 5376 and a minimum of 3592 collocations for the other 23 buoys). Finally, routine examination of wind speed histograms showed that a single buoy—44 011—acquired obviously unrealistic measurements throughout the WindSat period, and this buoy was thus also excluded from the validation analysis. The 22 selected buoy locations are shown in Fig. 1 and collocation statistics are given in Table I.

The present buoy selection approach differs from that of Freilich and Dunbar [7], who used the vector correlation between scatterometer and buoy measurements to identify representative buoys. Nonetheless, the buoys selected for these WindSat comparisons typically correlated well with the satellite measurements. The mean vector correlations of NESDIS0 data with the selected and unselected buoys were 1.53 and 1.01, respectively (the maximum possible vector correlation is 2.0). Among the selected buoys, Table I shows that buoy 42 002 in the Gulf of Mexico and three of the four buoys around Hawaii had notably small vector correlations; nonetheless, these buoys were included in the analysis. (For comparison, the buoys included in the Freilich and Dunbar analysis of NSCAT data [7] all had vector correlations exceeding 1.6.) The general tracking of vector correlation magnitude with centroid distance supports the assumption that collocation mismatches contribute measurably to differences between satellite and buoy data in the vicinity of coasts.

IV. BUOY COMPARISONS FOR NONRAIN-FLAGGED MEASUREMENTS

In this section, the accuracy of the highest quality NESDIS0 vector wind measurements is examined using the spatially and temporally collocated buoy data. The analysis considers only valid NESDIS0 measurements for which bit 2 of the EDR quality flag indicated no rain contamination. For comparison, all rain-free QuikSCAT vector wind measurements collected during the September–February period were collocated with the selected buoys and analyzed in the same way as the WindSat data. Although the QuikSCAT and NESDIS0 measurements were not necessarily collocated within 30 min and 50 km of each other (as each was with the buoy), the two satellites made measurements in the vicinity of the buoys at approximately the same local time, and thus would be expected to have sampled similar wind distributions over the six-month duration of the WindSat dataset.

Most users of the WindSat data will rely upon the single selected ambiguity provided in the WindSat EDR. However, ambiguity removal errors can result in large directional differences

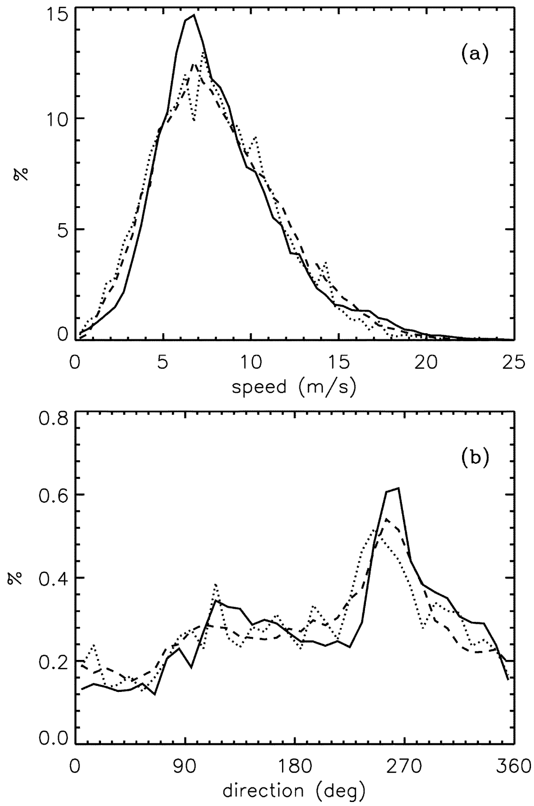

Fig. 2. Distributions of nonraining wind speed (a) and direction relative to north (b) from the NDBC collocated datasets. (Solid line) NESDIS0. (Dashed line) QuikSCAT. (Dotted line) NDBC 10-m neutral stability.

between collocated satellite and buoy measurements, thus complicating the interpretation of low-order directional comparison statistics. Following the approach of Freilich and Dunbar [7], two measures of directional accuracy were calculated for these buoy comparisons and for the global WindSat–QuikSCAT comparisons analyzed in Section V: 1) an indirect estimate of "ambiguity removal skill" or egregious directional errors based on the fraction of selected ambiguities that have directions that differ from that of the comparison (buoy or QuikSCAT) measurement by more than 90°; and 2) directional accuracy statistics for those selected ambiguities that are within 90° of the direction of the comparison data. The set of collocated wind velocity pairs after elimination of the "ambiguity removal" errors will be referred to as the "edited" data.

A total of 112 724 rain-free, valid, edited NESDIS0 wind estimates and 66 753 edited QuikSCAT measurements were analyzed, with wind speed and direction distributions shown in Fig. 2. While the NDBC and QuikSCAT wind speed histograms are similar, the NESDIS0 speed distribution is narrower for speeds less than 15 m/s; the NESDIS0 collocated dataset has relatively fewer winds with speeds less than 5 m/s or between 10 and 15 m/s than either the NDBC or QuikSCAT datasets. The NESDIS0 histogram flattens noticeably for wind speeds from 15–18 m/s, such that a larger fraction of NESDIS0 winds are greater than 16 m/s than in either of the other two datasets.

The directional histograms (wind direction relative to north, oceanographic convention) show greater differences between the datasets, although all three show a major concentration in the quadrant 225° to 315° (winds blowing from east to west) and a broad minimum near 45°. The $\sim 10°$ directional offset of the main peak between the NDBC and QuikSCAT data is consistent with previous findings that the NDBC buoy directions are rotated 8° to 10° counterclockwise relative to scatterometer and operational ECMWF and NCEP surface wind analysis products [7]. The NESDIS0 directional histogram is quite narrow near the maximum at 260°, falling off particularly rapidly as directions decrease (see discussion in Section V below). Simple low-order statistics of satellite-buoy speed and direction differences are given in Table II.

TABLE II
COMPARISON STATISTICS FOR THE "EDITED" SATELLITE VERSUS NDBC COLLOCATED DATASET

	NESDIS0	**QuikSCAT**
Speed rms (m/s)	1.43	1.22
Speed bias (m/s) [sat-buoy]	0.23	0.05
Directional Std. Dev. (°)		
(3-20 m/s)	25.2	18.7
(5-20 m/s)	21.5	16.7
Random Component Error		
Along-wind	1.0	0.75
Across-wind	2.8	2.0

Previous studies have demonstrated that vector wind estimates from many sources can be accurately characterized by an additive random component error model [6], [7], [11]. This error model naturally accommodates the nonnegative property of speeds, appropriately couples speed and direction errors at low true wind speeds, and replicates many of the observed properties of wind speed and direction comparison statistics. In particular, the random component error model quantitatively predicts both the observed positive bias of mean satellite wind speeds for small values of buoy wind speeds, and the increase in random differences between buoy and satellite wind directions with decreasing buoy wind speed.

Simulation-based numerical techniques have been developed for estimating the quantitative magnitudes of the random component errors from analyses of the speed dependence of satellite-buoy speed biases and directional standard deviations [6], [7]. Chelton and Freilich [11] reported QuikSCAT accuracies in terms of independent along- and across-wind additive random error component magnitudes based on coupled least squares fits of both speed biases and the standard deviations of QuikSCAT-NDBC directional differences [30].

Most previous analyses have assumed that the comparison buoy measurements were perfect, and thus all instrumental and representativeness errors were attributed to the satellite. In the present study, the simulation-based approach was extended to include random component errors in the buoy measurements as well as in the WindSat and QuikSCAT data. It was assumed throughout that the satellite data had unity gain and no offset relative to the NDBC measurements. Realizations of "true" wind velocities having Rayleigh distributed speeds and uniform directions were generated, to which were added separate along-wind and across-wind random component errors drawn from Gaussian distributions with specified standard deviations

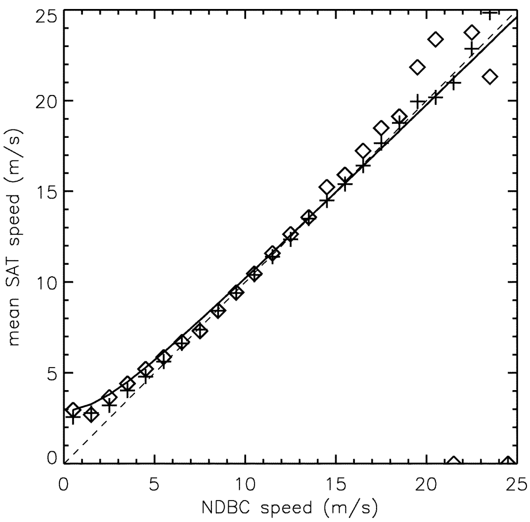

Fig. 3. Observed and simulated conditional mean satellite speeds binned on NDBC speeds from the collocated, "edited" dataset. (Diamonds) NESDIS0. (Crosses) QuikSCAT. (Solid line) NESDIS0 simulation using the best fit along- and across-wind random error component magnitudes of Table II. The dashed line represents unity gain and zero offset.

to simulate satellite and buoy measurements. The simulated noisy satellite measurements were then compared with the simulated noisy buoy measurements. Buoy random errors were taken to be 1 m/s in each component [11], and simulations were performed for a range of satellite component errors. Satellite component error magnitudes were estimated by minimizing the normalized square differences between simulated and observed wind speed biases and directional difference standard deviations for buoy speeds from 1–8 m/s [30].

Observed and simulated NESDIS0 and QuikSCAT mean wind speeds are shown in Fig. 3 as a function of collocated NDBC (10-m neutral stability) speed. Both satellite datasets had nearly unbiased wind speeds for NDBC speeds from ~5–15 m/s, and both exhibited the positive biases at low wind speeds characteristic of random component errors, with the NESDIS0 data having slightly larger low-buoy-speed biases. While the QuikSCAT measurements remained unbiased for NDBC speeds above 15 m/s, these buoy comparisons suggest that the NESDIS0 dataset increasingly overpredicts wind speed at high buoy speeds.

The fraction of satellite-buoy pairs having directional differences ("$\Delta\theta$") greater than $\pm 90^\circ$ decreased rapidly with increasing NDBC speed for both the NESDIS0 and QuikSCAT datasets (Fig. 4), qualitatively consistent with the prediction of the random component error model. The QuikSCAT data had relatively fewer large directional differences at all buoy wind speeds. The simulations underpredict the fraction of large differences for both satellite datasets, although the discrepancy between simulation and observations is much larger for the NESDIS0 measurements. Ambiguity removal errors (which are not accounted for in the random component error simulations) should cause the observed fraction of large differences to exceed the simulation predictions.

The standard deviation of $\Delta\theta$ for the edited collocated datasets (after removal of those collocations for which

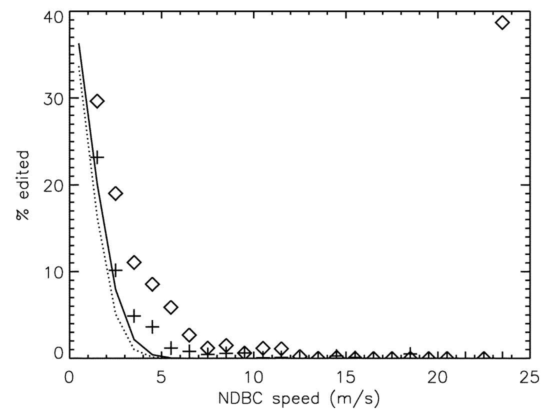

Fig. 4. Observed and simulated fractions of satellite-buoy directional differences exceeding $\pm 90^\circ$ in the unedited, collocated dataset. (Diamonds) NESDIS0. (Crosses) QuikSCAT. (Solid line) Simulation results for NESDIS0, using the random component errors from Table II. (Dotted line) Simulation results for QuikSCAT.

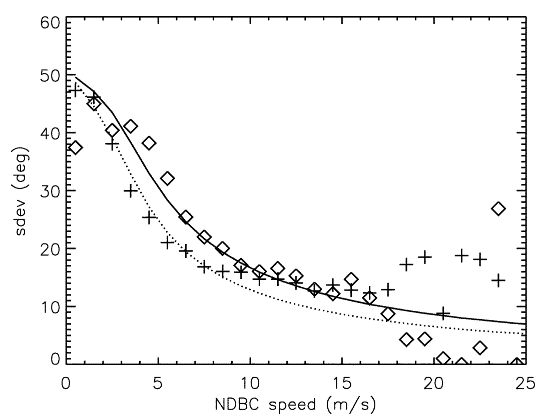

Fig. 5. Standard deviations of edited satellite-buoy directional differences. Symbols and line types as in Fig. 4.

$|\Delta\theta| > 90^\circ$) is shown in Fig. 5 as a function of NDBC speed. The simulation based on the best fit along- and across-wind random component error magnitudes (Table II) is quantitatively similar to the NESDIS0 observations for NDBC wind speeds less than 17 m/s, notwithstanding the fact that the fit was performed only for wind speeds less than 8 m/s. The NESDIS0 performance exceeded that predicted by the simulation for higher wind speeds (although there were very few high wind speed observations in the collocated NDBC dataset). QuikSCAT-buoy directional differences are consistent with the simulation predictions for NDBC speeds below ~9 m/s; at higher buoy wind speeds, the QuikSCAT directional performance was worse than predicted by the random component error model, qualitatively similar to the NSCAT results [7]. The NESDIS0 directional accuracy was generally worse than that of QuikSCAT for wind speeds below 12 m/s, consistent with the larger NESDIS0 random component error. The two instruments had comparable performance in the speed range from 12–16 m/s, and the NESDIS0 accuracy relative to the buoys was better for higher wind speeds.

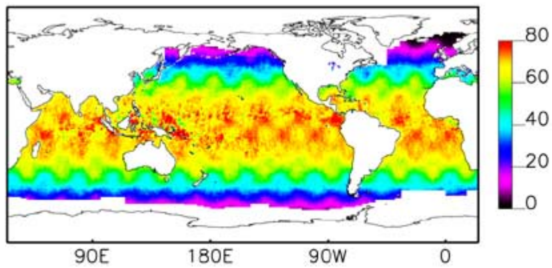

Fig. 6. Fraction of rain-free NESDIS0 WindSat data for which there was a collocated QuikSCAT measurement.

V. Global Characterization From QuikSCAT Comparisons

Comparisons with QuikSCAT measurements can be used to extend the regional, buoy-based WindSat validation of Section IV to the entire global ocean, covering a much wider range of wind and atmospheric conditions. Although issues of resolution and temporal/spatial collocation differences remain in WindSat–QuikSCAT comparisons, each of the satellite datasets corresponds to a near-instantaneous spatial average of the wind field. Representativeness errors caused by the difference between instantaneous spatial averages and point temporal averages are thus eliminated in the satellite–satellite comparisons.

A. Global WindSat–QuikSCAT Dataset

As with the NDBC comparisons, only QuikSCAT wind measurements from the nadir and sweet zones were used for the global analysis. Similarly, only NESDIS0 vector wind estimates for which EDR quality flag bits 4–27 and bit 29 were not set were considered. Comparisons were made between the selected ambiguity from each dataset.

The global collocated dataset was constructed by identifying all QuikSCAT vector wind solutions within 50 km and 1 h of each qualifying NESDIS0 vector wind solution. If QuikSCAT measurements from two different revs satisfied the 1-h temporal threshold, only data from the rev closest in time to the WindSat measurement were considered. (QuikSCAT "revs" are orbits defined to begin and end over land near the South Pole.) When several 25-km QuikSCAT measurements from the same rev satisfied the spatial cutoff criterion, the QuikSCAT measurement closest to the WindSat measurement location was used. In order to focus on the highest quality satellite measurements, the global comparisons presented in this section exclude any collocated measurement pair for which either the QuikSCAT (MUDH) autonomous rain flag, or the NESDIS0 (EDR bit 2) rain flag was set.

A total of 99 933 671 rain-free, collocated measurement pairs were obtained over the September–February period, although not all of these pairs were independent owing to the difference in grid resolution between the WindSat (12.5 km) and QuikSCAT (25 km) datasets. As shown in Fig. 6, QuikSCAT comparison measurements were generally available for more than 70% of all rain-free WindSat data within 30° of the equator. The number of collocations decreased at higher latitudes—even after accounting for the latitudinal dependence of ocean surface area—because the WindSat and QuikSCAT terminator orbits have opposite sense. The WindSat ascending node is near 1800 hours local time, while the QuikSCAT ascending node is ∼0600, and thus the time difference between spatially collocated QuikSCAT and WindSat measurements tended to increase with increasing latitude.

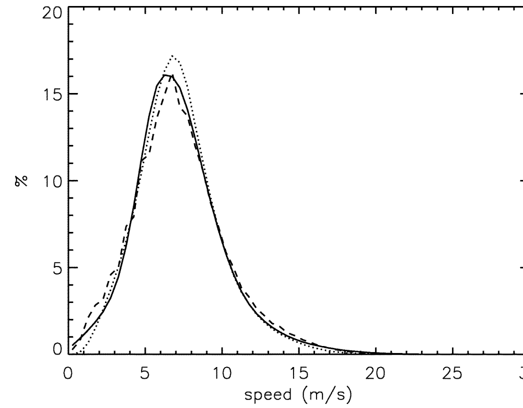

Fig. 7. Wind speed histograms from the global, collocated dataset. (Solid line) NESDIS0. (Dashed line) QuikSCAT. (Dotted line) Interpolated NCEP 10-m wind analyses.

TABLE III
LOW-ORDER WIND SPEED STATISTICS FOR THE GLOBAL COLLOCATED DATASET

	Mean	**Std. Dev.**
Windsat	7.24	2.94
QuikSCAT	7.23	3.04
NCEP	7.22	2.68

B. WindSat Accuracy From the Global QuikSCAT Comparisons

The NESDIS0 and QuikSCAT wind speed histograms from the global collocated dataset are shown in Fig. 7, and the low-order speed statistics are given in Table III. (The NCEP distribution was obtained by trilinearly interpolating the scalar 10-m wind speeds from the operational NCEP global analyses to the locations and times of the QuikSCAT measurements.) The satellite wind distributions had nearly identical means and their standard deviations differed by only 0.1 m/s. Although the NCEP distribution had a negligibly smaller mean, the NCEP standard deviation was 10% smaller than either the NESDIS0 or QuikSCAT datasets. There were relatively more QuikSCAT than NESDIS0 winds in the bands 0–4 and 10–16 m/s, consistent with the buoy results (Fig. 2).

The NESDIS0 dataset had more very high winds than either of the other datasets. There were 822 NESDIS0 collocated speeds larger than 49.9 m/s, compared with a maximum QuikSCAT speed of 39.4 m/s. Some 512 (62%) of these NESDIS0 speeds were collocated with QuikSCAT speeds below 5 m/s, and 284 large NESDIS0 speeds were associated with QuikSCAT measurements between 5 and 10 m/s. As none of the 50-m/s NESDIS0 speeds was associated with QuikSCAT measurements exceeding 17 m/s, it seems likely that these

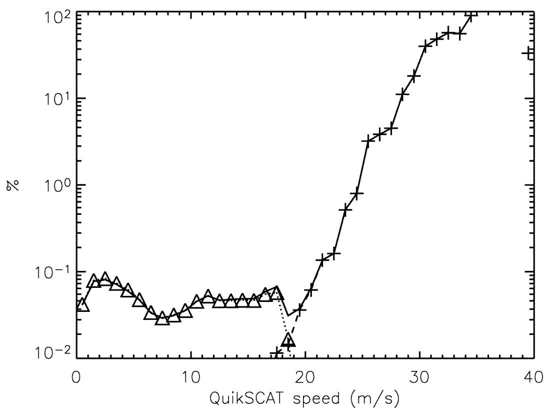

Fig. 8. Fraction of all global collocations for which the speed difference exceeded ± 10 m/s, as a function of QuikSCAT speed. (Triangles) NESDIS0-QuikSCAT >10 m/s. (Crosses) NESDIS0-QuikSCAT < -10 m/s.

WindSat solutions are erroneous and they were excluded from all remaining calculations.

The overall rms difference between the collocated NESDIS0 and QuikSCAT speeds was 1.04 m/s. Although generally Gaussian-shaped, the distribution of speed differences (not shown) had thicker tails than a normal distribution: 0.4% of the NESDIS0-QuikSCAT speed differences exceeded 3.12 m/s (approximately three standard deviations from the mean), while 0.7% of the differences were less than -3.12 m/s (compared with 0.14% for a Gaussian).

For the entire global collocated dataset, only 0.04% of all the speed differences exceeded ± 10 m/s. Fig. 8 reveals that while fewer than 0.1% of all pairs with QuikSCAT speeds less than 21 m/s had (unsigned) speed differences of 10 m/s or larger, the percentage of large speed differences increased rapidly with increasing QuikSCAT wind speed. Indeed, for collocated pairs in which QuikSCAT speeds exceeded 31 m/s, more than 50% of all NESDIS0 measurements were smaller than the QuikSCAT speed by more than 10 m/s.

Mean NESDIS0 speeds binned on QuikSCAT speeds are presented in Fig. 9, along with simulated results based on the NESDIS0 and QuikSCAT random component error magnitudes calculated from the buoy comparison. As in Section IV, the simulation was constructed by generating a Rayleigh-distributed "true" wind field with uniform directions, then adding (separate) realizations of along-wind and cross-wind random component errors to generate realizations of WindSat and QuikSCAT measurement pairs. The observed comparisons and the simulation are almost identical for QuikSCAT wind speeds from 4–20 m/s. This speed range accounts for $\sim$88% of both the global and buoy collocations. Conditional mean NESDIS0 speeds remained almost unbiased for QuikSCAT speeds below 4 m/s, in mild contrast with the predictions of the random component error model. For QuikSCAT wind speeds above 20 m/s, the observations and simulation diverged, with NESDIS0 conditional mean speeds increasingly biased low with increasing QuikSCAT wind speed. This observed tendency toward NESDIS0 low bias is much larger than the simulation predicts, and while it is consistent with the results of Fig. 8, it appears to contradict the results of the buoy analyses shown in Fig. 3. The value of the global comparison becomes evident when it is noted that only 121 WindSat–NDBC collocations had NDBC speeds greater than 20 m/s, while there were nearly 1×10^5 valid WindSat–QuikSCAT collocations with QuikSCAT speeds in this speed range.

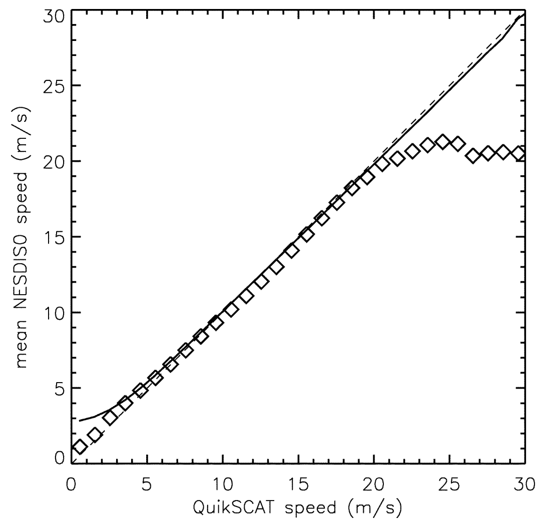

Fig. 9. Conditional mean NESDIS0 wind speeds as a function of QuikSCAT speed from the global collocated dataset. (Diamonds) Observations. (Solid line) Simulation based on NESDIS0 and QuikSCAT random component error magnitudes from Table II. (Dashed line) Perfect agreement, slope $= 1$.

Directional differences can be caused by random component errors (especially important at low true wind speeds) and by ambiguity removal errors. In principle, ambiguity removal errors will increase the fraction of satellite–satellite directional differences exceeding a particular threshold for moderate and high wind speeds, while the existence of alternate ambiguities (which themselves are contaminated by random component errors) can decrease the fraction of large directional differences at low wind speeds. The observed fraction of global collocated pairs with $|\Delta\theta| > 90^\circ$ matches well with simulations based on the NESDIS0 and QuikSCAT random component error magnitudes of Section IV and neglecting ambiguity removal errors (Fig. 10). Consistent with the presence of a small number of ambiguity removal errors and the NDBC results (Fig. 4), large observed directional differences occurred slightly more frequently than predicted by the simulation.

Standard deviations of directional differences as a function of wind speed are shown in Fig. 11 for both observations and simulations. For QuikSCAT wind speeds less than $\sim$12 m/s, there was general agreement between the observations and the simulations based on random component error magnitudes calculated from the NDBC comparisons, although at moderate wind speeds, the edited observations tended to have smaller $\Delta\theta$ variability than predicted. At higher wind speeds, the observed standard deviations did not decrease with increasing wind speed as predicted by the simulation, and indeed the difference standard deviations began to increase for QuikSCAT speeds above 20 m/s. This global result is qualitatively consistent with the NDBC comparisons (Fig. 5) and may be due to QuikSCAT direction errors. This high wind speed feature of the scatterometer directions likely results from selection of incorrect wind direction solutions that do not, however, differ from the correct solution by more than the 90° editing criterion.

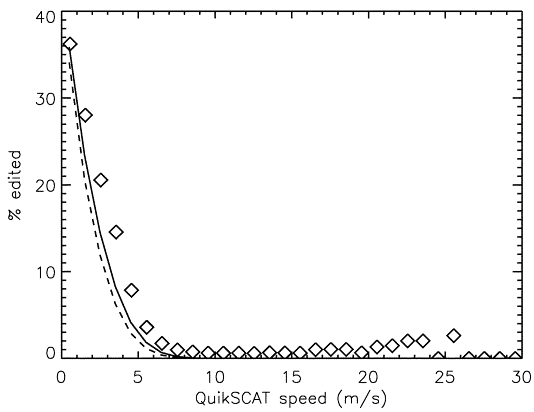

Fig. 10. Fraction of large ($> 90°$) |QuikSCAT-NESDIS0| directional differences as a function of QuikSCAT speed. (Diamonds) Observations. (Solid line) Simulation based on along- and across-wind random component errors calculated from the global collocated dataset. (Dashed line) Simulation based on random component errors calculated from Table II.

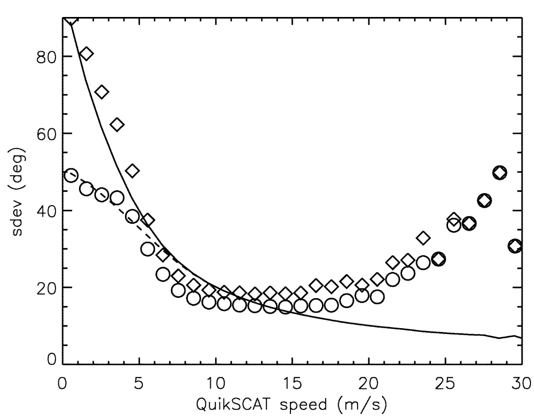

Fig. 11. Observations and simulations of the standard deviation of $\Delta\theta$ between global, collocated QuikSCAT and NESDIS0 measurements, as a function of QuikSCAT wind speed. (Diamonds) Observations (no directional editing). (Circles) After removal of collocated pairs for which $|\Delta\theta| > 90°$. (Solid line) Best fit simulation to the unedited observations using the buoy-derived NESDIS0 and QuikSCAT along-wind and across-wind error magnitudes from Table II. (Dashed line) Simulation after directional editing.

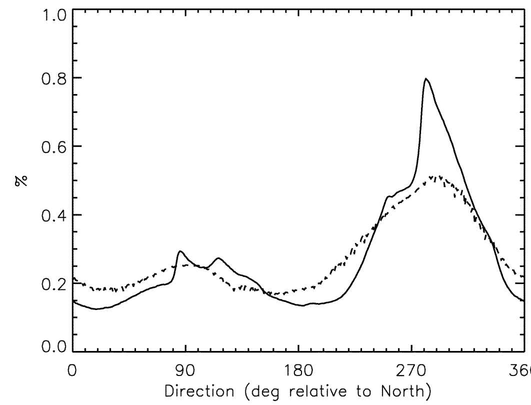

Fig. 12. Directional distributions (relative to north) for rain-free data from the global WindSat–QuikSCAT collocated dataset. (Solid line) NESDIS0. (Dotted line) QuikSCAT.

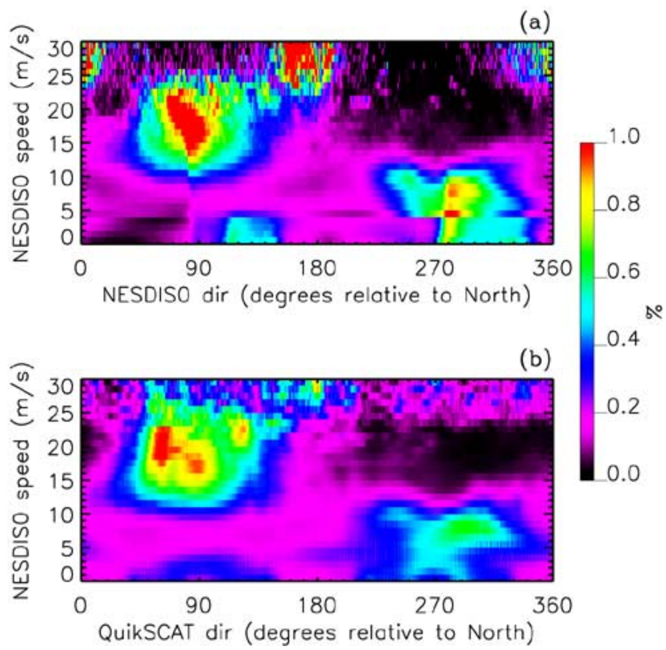

Fig. 13. Directional histograms from the global collocated dataset, for NESDIS0 speeds from 0–30 m/s. The histogram is normalized to have unity area at each wind speed (thus removing the effects of the wind speed distribution). The NESDIS0 wind speed was used as a parameter for both panels. (Top panel) NESDIS0 directions. (Bottom panel) QuikSCAT directions.

Examination of the separate QuikSCAT and NESDIS0 wind direction distributions from the collocated data (Fig. 12) illuminates weaknesses in the NESDIS0 vector wind retrievals. While the directional histograms from each dataset were dominated by the tradewinds (directions near 270° in the oceanographic convention used here) with a subsidiary concentration for the midlatitude westerlies around 90°, the NESDIS0 distribution is much more concentrated than the QuikSCAT data in a narrow peak near 280°, and there were fewer WindSat directional retrievals in broad bands corresponding to northerly and southerly winds. The discrepancies remain when wind directions in each dataset were referenced relative to the spacecraft velocity vector (not shown).

The two-dimensional normalized directional histograms for the NESDIS0 and QuikSCAT global, collocated measurements are roughly similar (Fig. 13). Data from each instrument showed a relative concentration of easterly winds (directions 230° to 350° for NESDIS0 speeds less than 10 m/s), with westerlies dominating for wind speeds from 10–25 m/s. However, the NESDIS0 directional histogram is characterized by discontinuities and unrealistic features that are not present in the QuikSCAT histogram. A notable discontinuity appears in the NESDIS0 distribution between 4 and 5 m/s at all directions. The NESDIS0 histograms are unrealistically concentrated at 270° to 290° (consistent with the sharp peak in the one-dimensional histogram of Fig. 12). A discontinuity in direction at 70° to 90° is evident for NESDIS0 at speeds below 20 m/s, with few selected directions between 0° to 90° at low wind speeds, and a relative concentration of measurements at slightly larger directions. NESDIS0 directions for speeds above 25 m/s were concentrated near 0° and 180°.

VI. Accuracy of NESDIS0 Rain-Flagged Measurements

Large quantities of atmospheric liquid water and rain present challenges for wind retrieval from microwave radiometers and scatterometers [21], [31]–[34]. Extensions to the nonraining backscattering and radiative transfer models are required to account for scattering from water droplets in the atmosphere and centimetric roughness caused by rain drops hitting the ocean surface.

Accurate wind retrievals are not possible at all in heavy rain, so these measurements must be identified and excluded from ambiguity removal and subsequent geophysical analyses. The NESDIS0 dataset has a rain flag (bit 2 of the EDR quality flag) that was set during ground processing, based on comparisons between vertical and horizontal polarization T_b differences at 37 GHz, differences between vertical polarization T_b at 37 and 18 GHz, or absolute values of the horizontal polarization T_b at 18 and 37 GHz [14].

The regional impact of the NESDIS0 rain flagging is evident in six-month coverage comparisons (Fig. 14). As the two instruments have different nominal in-swath spatial sampling, coverage here was defined in terms of the number of orbits ("passes") for which at least one nonrain-flagged valid wind was retrieved in a given $1^\circ \times 1^\circ$ area. Sampling was more frequent (by approximately a factor of 2) for QuikSCAT relative to WindSat, since the 1700-km QuikSCAT swath is much wider than the 895-km effective WindSat swath. Sampling increased with increasing latitude for each instrument; for the 1700-km-wide QuikSCAT swath, consecutive orbits overlap at latitudes poleward of 50°. Both the top and middle panels of Fig. 14 show regional sampling differences that are generally consistent with rain climatology, with sampling significantly diminished over the western Pacific warm pool and in the Intertropical and the South Pacific Convergence Zones. However, the regional differences are larger on a fractional basis for the NESDIS0 dataset.

The bottom panel of Fig. 14 shows the fraction of nonraining QuikSCAT passes for which there was a collocated (nonraining) NESDIS0 WindSat pass. Typically far fewer than 40% of QuikSCAT passes in any $1^\circ \times 1^\circ$ area were collocated with WindSat passes, in part due to the differing instrumental swath widths. However, in contrast with Fig. 6 (in which there was no systematic, large-scale longitudinal variation in the fraction of rain-free WindSat measurements that were collocated with rain-free QuikSCAT solutions), there are definite regional features in the fraction of WindSat collocations with rain-free QuikSCAT measurements. Relatively more collocations were found in the drier eastern portions of the midlatitude Southern Hemisphere oceans, while there were significantly fewer collocations in the climatologically rain-prone areas of the convergence zones and the tropical warm pool. In these latter regions, the bottom panel of Fig. 14 suggests that WindSat measurements were flagged for rain more frequently than were spatially and temporally collocated QuikSCAT measurements. Overly conservative rain flagging can seriously degrade the quality of satellite wind fields, since there are significant correlations between rain and important wind forcing features such as strong synoptic-scale cyclones [35].

Comparisons with SSM/I measurements at the NDBC buoy locations confirmed that the NESDIS0 data were overflagged for rain. Rain rates are routinely calculated from the SSM/I microwave radiometer instruments on the operational Defense Meteorological Satellite Program (DMSP) spacecraft

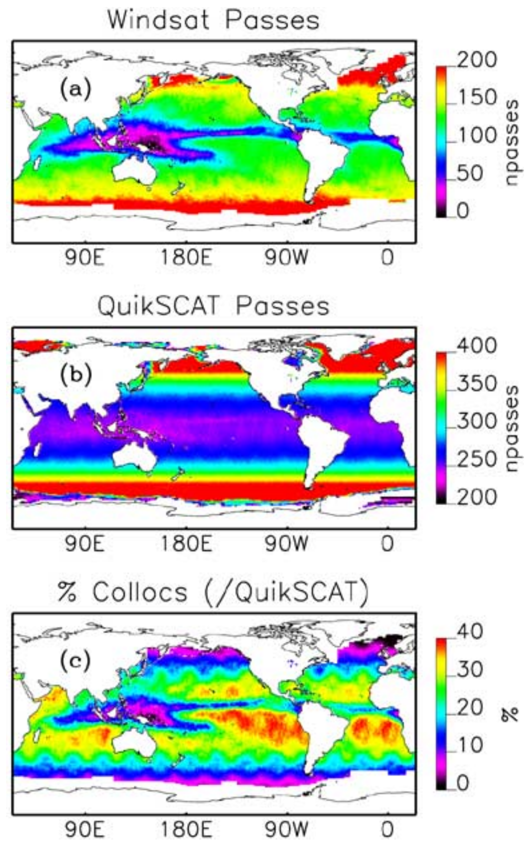

Fig. 14. Coverage maps for (top panel) nonraining WindSat and (middle panel) QuikSCAT datasets over the six-month dataset. Colors indicate number of passes in each $1^\circ \times 1^\circ$ area. (Bottom panel) Fraction of all QuikSCAT passes for which there is a collocated WindSat pass in the NESDIS0 dataset.

[31], and the F13 DMSP satellite has 0600 and 1800 local equatorial crossing times. Thus, although there was only a relatively small number of NDBC collocations for which both SSM/I and WindSat rain-contaminated data were acquired nearly simultaneously at the buoys, the local times for all F13 SSM/I collocations with the NDBC buoys were similar to those of WindSat. Approximately 14.3% of otherwise valid WindSat–NDBC collocations at the 22 selected buoys had the rain flag set, but only 8.1% of the SSM/I measurements had nonzero rain rate for the September–February time period.

The distributions of rain flagged data as a function of NDBC wind speed are shown in Fig. 15 for both the NESDIS0 and F13 SSM/I collocated datasets. The NESDIS0 and SSM/I data both had rain flags set in ~5% of the collocations for which NDBC speeds were less than 7 m/s. However, an increasingly greater fraction of NESDIS0 measurements (compared with SSM/I) was flagged for rain for NDBC speeds above 7 m/s. More than half of all collocated NESDIS0 measurements corresponding to NDBC wind speeds above 17 m/s were flagged as rain-contaminated and more than 60% of all collocated NESDIS0 data were rain-flagged for NDBC wind speeds greater than 19 m/s, while at most ~30% of the SSM/I collocations had nonzero rain rates.

The accuracies of the rain-flagged WindSat are compared in Figs. 16–18 with those from the (more numerous) non-rain-flagged data discussed in Section IV above. Except for NDBC wind speeds between 1 and 2 m/s, a larger fraction of

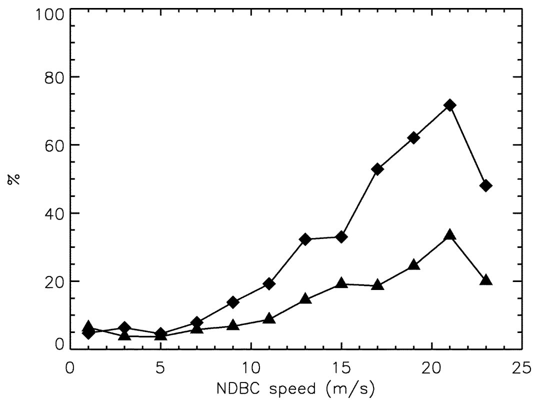

Fig. 15. Fraction of collocated data flagged for rain as a function of NDBC speed. (Diamonds) NESDIS0. (Triangles) F13 SSM/I measurements with nonzero rain rates.

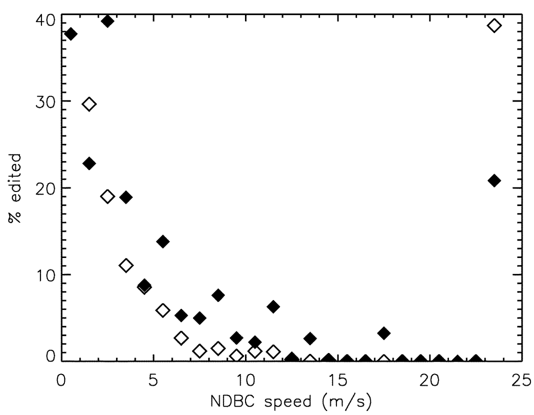

Fig. 16. Fraction of NESDIS0–NDBC pairs with $|\Delta\theta| > 90^\circ$ for (open symbols) nonraining and (filled symbols) raining conditions.

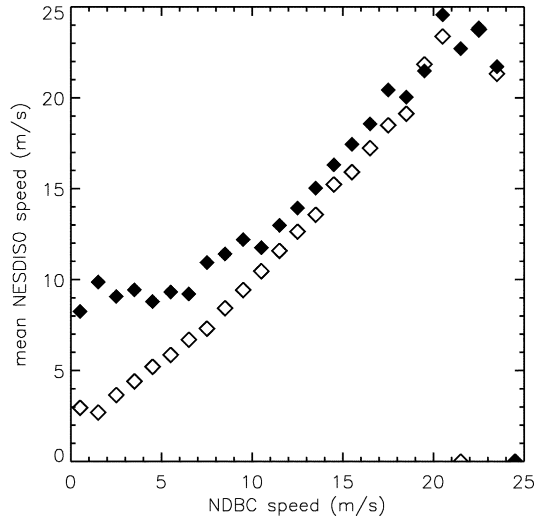

Fig. 17. Conditional mean NESDIS0 (open symbols) nonraining and (filled symbols) rain-flagged speeds from the collocated NDBC dataset.

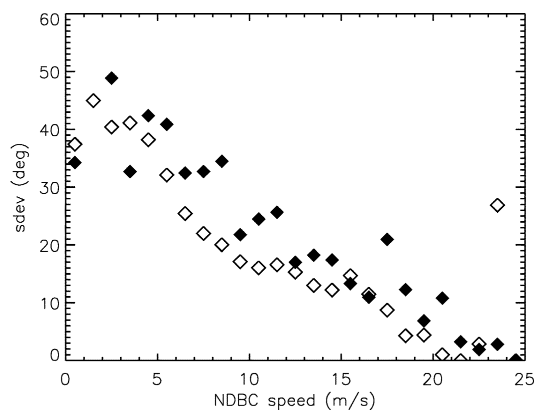

Fig. 18. Standard deviations of edited NESDIS0 minus NDBC directional differences for (open symbols) nonraining and (filled symbols) raining collocated data.

rain-flagged NESDIS0 directions differed from the buoy-measured directions by more than 90° than was the case for the nonrain-flagged NESDIS0 data (Fig. 16). For NDBC wind speeds greater than ~11 m/s, the rain-flagged data had only slightly larger speed biases than did the nonflagged measurements (Fig. 17). However, for lower NDBC speeds, the rain-flagged NESDIS0 measurements exhibited increasingly larger positive speed biases with decreasing NDBC speed, in contrast with the results from the nonrain-flagged measurements; indeed, the bin-averaged rain-flagged NESDIS0 speeds showed little sensitivity to the collocated NDBC speed for NDBC speed less than about 8 m/s.

The directional error characteristics of rain-flagged NESDIS0 data were similar to those of the nonrain-flagged data for NDBC wind speeds under about 5 m/s (Fig. 18). As with the nonrain-flagged data considered in Section IV, the standard deviations of the NESDIS0-NDBC directional differences for rain-flagged data decreased rapidly with increasing NDBC wind speed; however, the rain-flagged WindSat directions had larger errors for wind speeds exceeding 5 m/s.

The SSM/I comparisons and speed bias results are consistent with an overly conservative rain flag, especially at higher wind speeds. It appears that rain effects erroneously increased the reported NESDIS0 wind speed (especially at low true wind speeds), and that the NESDIS0 data may have been properly flagged for low true (NDBC) wind speeds. For NDBC wind speeds exceeding 10 m/s, the NESDIS0 rain flag may have been improperly set a significant fraction of the time (although it should be noted that the directional accuracy of the rain-flagged data, even for high NDBC speed, was worse than for the nonrain-flagged data).

VII. Second-Generation WindSat Vector Wind Dataset

The B1 vector winds were collocated with the selected NDBC buoys and subjected to the same analyses as were presented in Sections IV and VI above. The presence of two rain flag bits based on different (not necessarily complementary) criteria complicated the analysis and allowed different "rain-free" and "rain-contaminated" subsets to be defined. One of the rain flags (here denoted the "SDR" flag) is based on direct T_b measurements and is similar to the NESDIS0 rain flag. The second ("EDR") flag is set based on a combination of T_b and retrieval misfit values as described in [17]. In general, the SDR flag was set significantly more often than the EDR flag and the SDR flag was set nearly every time that the EDR flag was set. The highest

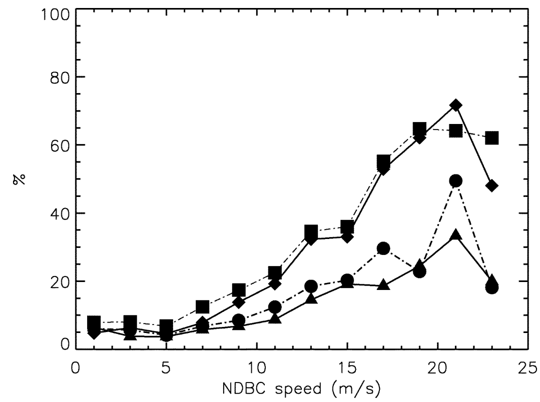

Fig. 19. Rain flagging as in Fig. 15 for (diamonds) the NESDIS0, (squares) B1 SDR + EDR raining, (circles) B1 EDR-only raining, and (triangles) SSM/I F13 datasets collocated with the NDBC buoys.

quality B1 measurements presumably result from requiring that neither the SDR nor the EDR flag be set (denoted here as the "SDR + EDR clear" dataset). A second (possibly) nonraining dataset was defined by requiring only that the EDR flag not be set (the "EDR-only clear" dataset). The "SDR + EDR raining" and "EDR-only raining" subsets are the complements of the "clear" datasets.

Fig. 19 shows the wind speed dependence of the SDR + EDR and EDR-only flagging compared with the F13 SSM/I collocations as in Fig. 15. The wind speed dependence of the B1 SDR + EDR rain flag was nearly identical to that of the NESDIS0 rain flag. This is not surprising, since the EDR rain flag bit was set almost every time the SDR bit was set, and the SDR bit logic is similar to that of the NESDIS0 rain flag bit (overall, the SDR + EDR rain flag was set for 17.4% of the valid B1 collocations, compared with 14.3% for the NESDIS0 rain flag). The EDR-only rain flag was set for 9.5% of the valid collocations (compared with 7.9% rain occurrence rate for the F13 SSM/I collocations). The wind speed dependence of the EDR-only flag was similar to that of the SSM/I flag. If the wind speed and direction accuracies of the B1 EDR-only clear data are acceptable, the sampling problems caused by NESDIS0 overflagging (evident in the middle and bottom panels of Fig. 14) might be alleviated in the B1 dataset if the EDR flag alone is used to differentiate raining from nonraining measurements.

Wind speed and direction histograms for the B1 clear datasets are compared with the distributions for NDBC and NESDIS0 nonraining measurements in Fig. 20. The B1, QuikSCAT, and NDBC speed histograms were nearly identical for wind speeds up to the peak of the distribution (near 7 m/s), suggesting that the B1 datasets might represent an improvement on the NESDIS0 dataset (which was depleted in low wind speeds). However, both of the B1 distributions exhibited an unrealistic peak at 10–11 m/s, bracketed by similarly unrealistic minima at 8–9 and 11–13 m/s; these features were not present in the NESDIS0, QuikSCAT, or NDBC datasets.

The B1 datasets had nearly identical directional distributions (bottom panel in Fig. 20), and in general were more similar to the QuikSCAT histogram than was the NESDIS0 curve. In particular, the B1 directional distributions did not exhibit the sharp decrease near 245° and the deep local minimum seen in the NESDIS0 histogram for directions 180° to 240°.

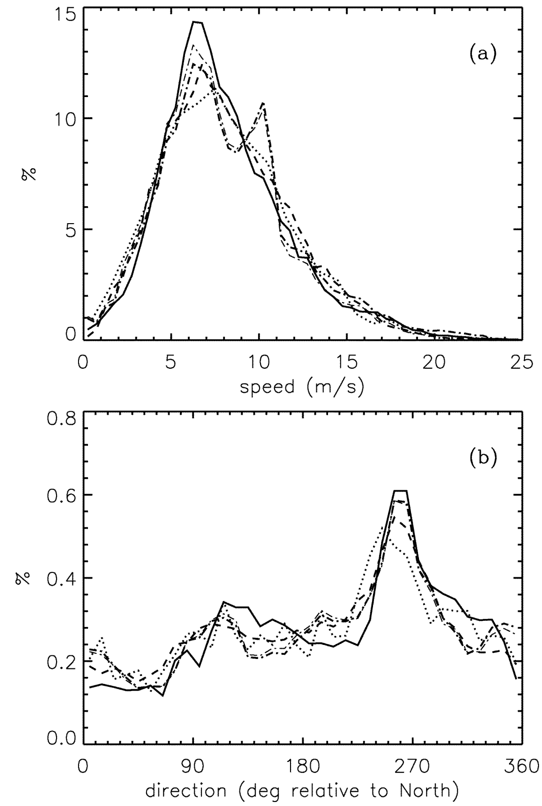

Fig. 20. (a) Observed wind speed and (b) wind direction distributions for the nonraining satellite and NDBC collocated datasets (as in Fig. 2). (Solid line) NESDIS0. (Light dashed–dotted line) B1 SDR + EDR clear. (Heavy dashed–dotted line) B1 EDR-only clear. (Dashed line) QuikSCAT. (Dotted line) NDBC.

TABLE IV
COMPARISON STATISTICS FOR THE "EDITED" B1 VERSUS NDBC NONRAINING, COLLOCATED DATASETS

	SDR+EDR Clear	**EDR-only Clear**
Speed rms (m/s)	1.29	1.52
Speed bias (m/s) [sat-buoy]	0.17	0.30
Directional Std. Dev. (°)		
(3-20 m/s)	23.9	23.9
(5-20 m/s)	21.0	21.2
Random Component Error		
Along-wind	0.75	0.75
Across-wind	2.6	2.6

Low-order buoy–satellite comparison statistics for the B1 nonraining datasets are given in Table IV. The B1 accuracy was comparable to or slightly better than the NESDIS0 measurements (Table II). The EDR-only dataset had only slightly worse speed bias and rms statistics than did the EDR+SDR dataset, and comparable directional statistics.

Speed bias and directional differences as a function of buoy speed for the nonraining B1 datasets are compared with QuikSCAT and NESDIS0 results in Figs. 21 and 22. The two B1 datasets had virtually identical performance for wind speeds up to 22 m/s (Fig. 21; there were only 68 collocations for larger buoy speeds). For wind speeds below 15 m/s, the B1 speed biases were the same as those for QuikSCAT, while

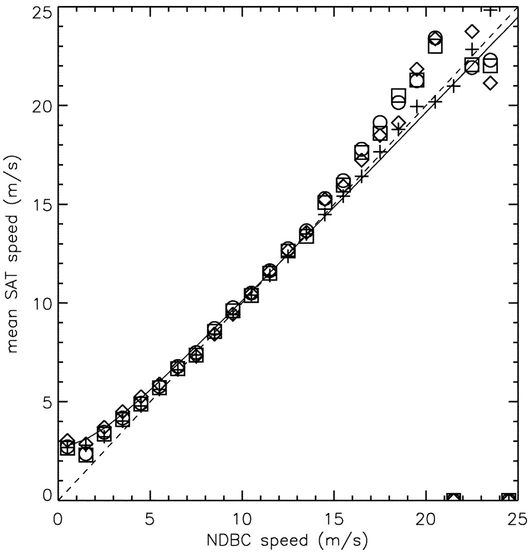

Fig. 21. (Symbols) observed and (line) simulated wind speed biases for the nonraining edited NDBC collocated data. (Diamonds) NESDIS0. (Crosses) QuikSCAT. (Squares) B1 SDR + EDR clear. (Circles) B1 EDR-only clear. The simulation was based on random component error magnitudes from Table IV.

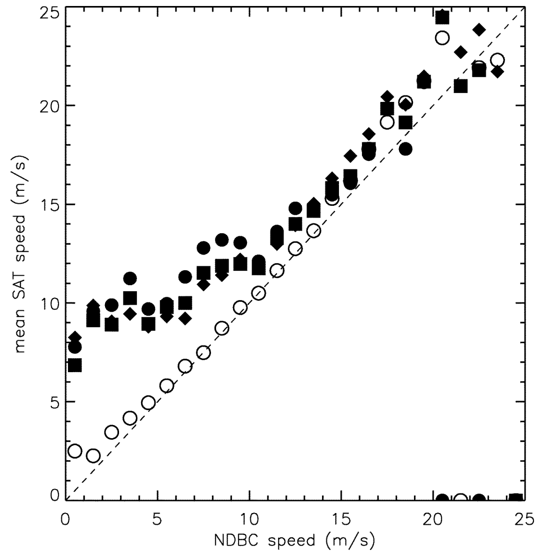

Fig. 23. Wind speed bias comparisons for (filled symbols) rain-flagged WindSat measurements, compared with (open circles) rain-free B1 EDR-only clear data. Symbol shapes are defined as in Fig. 21.

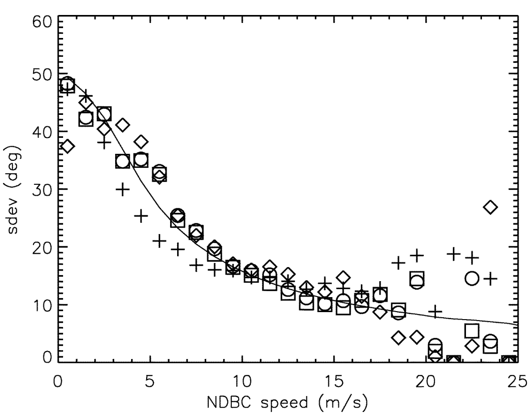

Fig. 22. As in Fig. 21 but for satellite-buoy direction difference standard deviations.

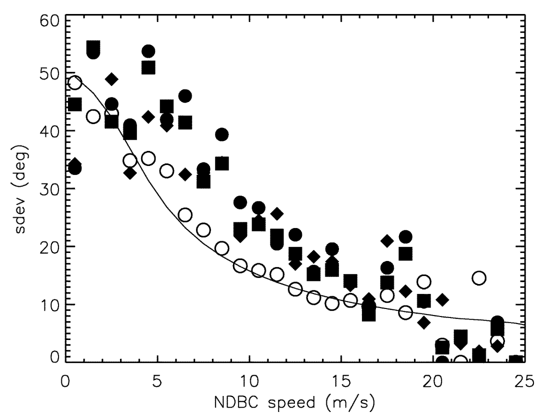

Fig. 24. As in Fig. 23 but for satellite-buoy direction difference standard deviations.

for higher NDBC speeds, the B1 speeds were larger than the buoy speeds, consistent with the NESDIS0 buoy comparison results (Fig. 3). The directional accuracies of the B1 datasets were slightly better than those of NESDIS0 for wind speeds below 15 m/s, although the QuikSCAT accuracy was uniformly better than any of the WindSat datasets for speeds less than 10 m/s. In the wind speed range 10–15 m/s, all of the datasets had quantitatively similar performance. At higher NDBC wind speeds, QuikSCAT accuracy decreased and NESDIS0 accuracy increased as discussed in Section IV, while B1 datasets had generally intermediate directional accuracy.

Wind speed biases and directional accuracies for the two B1 rain-flagged datasets are compared with the B1 EDR-only clear measurements in Figs. 23 and 24. The presence of rain caused the B1 speed estimates to be biased high for NDBC wind speeds under 15 m/s, consistent with the NESDIS0 results discussed in Section VI above. For NDBC speeds above 15 m/s, the rain-flagged data had negligible additional bias compared with the rain-free B1 EDR-only clear data (open circles). The B1 SDR + EDR rain-flagged data had nearly the same bias as the rain-flagged NESDIS0 measurements for "low" NDBC speeds (<15 m/s), since both the B1 SDR and the NESDIS0 rain flag bits were set based on similar T_b threshold criteria. In this speed range, the B1 EDR-only rain-flagged measurements had larger mean bias than did the measurements for which the SDR + EDR flag bit was set. As noted above, the EDR-only raining data were a subset of the SDR + EDR rain-flagged measurements, and the comparisons with SSM/I data suggested that the SDR + EDR rain flag was set too frequently at all speeds, although the discrepancy was especially large for NDBC wind speeds exceeding 7 m/s (Fig. 15). The results of Fig. 23 imply that the effect of rain contamination is to erroneously increase the wind speed reported by WindSat; since the SDR + EDR raining dataset included measurements incorrectly flagged for rain (and thus *not* actually contaminated), the mean bias of the SDR + EDR raining dataset was smaller than that of the EDR-only raining measurements (for which a larger fraction were truly rain-contaminated).

The directional accuracy of the rain-flagged measurements for all WindSat datasets improved with increasing NDBC wind speed, but was everywhere worse than the accuracy of the nonraining data (Fig. 24) except for noisy, sparsely sampled speeds above 20 m/s. As with the speed bias results of Fig. 23, the directional accuracy of rain-flagged data became similar to (although generally slightly worse than) that of the nonflagged (presumably rain-free) measurements for buoy speeds above 15 m/s.

VIII. Conclusion

WindSat is the first spaceborne demonstration of ocean surface wind speed and direction measurement using polarimetric microwave radiometry. As this approach will be used to make operational measurements of wind velocity on the U.S. National Polar-orbiting Environmental Satellite System (NPOESS) constellation starting in the 2010 time frame, it is essential to quantify the wind performance of polarimetric radiometers, both to improve processing algorithms and to prepare for future interpretation and assimilation of the NPOESS wind measurements.

Two, six-month (September 1, 2003–February 28, 2004) global vector wind datasets—denoted here as "NESDIS0" [12]–[14] and "B1" [17]—were validated in this study through comparison with measurements from 22 selected NDBC buoys and with global collocations with the QuikSCAT scatterometer. The two WindSat products resulted from processing different versions of the basic radiometer T_b measurements, using different empirical model functions and different retrieval algorithms. Comparisons of the accuracies of the two products indicate the potential for future improvements in radiometer-based wind velocity measurements.

The key statistical measures of rain-free accuracy from buoy comparisons are summarized in Tables II (for NESDIS0) and (for the B1 datasets). Over the wind speed range 3–20 m/s, the WindSat products had speed biases of 0.23 m/s (NESDIS0) and 0.30 m/s (B1, using only the EDR rain flag bit to identify rain-contaminated data), compared with a QuikSCAT bias of 0.05 m/s for the buoy collocations in this same time period. Rain-free satellite-buoy rms speed differences were 1.43 m/s (NESDIS0), 1.52 m/s (B1), and 1.22 m/s (QuikSCAT); the standard deviations of directional differences (for wind speeds 3–20 m/s) were 25.2° (NESDIS0), 23.9° (B1), and 18.7° (QuikSCAT). Based on these metrics, the preliminary WindSat vector wind measurements are somewhat less accurate than those of the QuikSCAT scatterometer, with the more recent B1 data product being slightly more accurate than the NESDIS0 dataset. (A subsequent refinement of the NESDIS0 product was made available too late to be validated in this study; results for this product will be reported elsewhere.) Comparisons of buoy, QuikSCAT, and B1 wind speed histograms showed that the rain-free B1 datasets had an unrealistic local peak near 10-m/s speeds (Fig. 20), suggesting a minor model function or retrieval algorithm error.

The rain-free WindSat measurements are well characterized in terms of additive random component errors, with different along-wind and cross-wind magnitudes. Indeed, the buoy comparisons presented here demonstrate that the WindSat direction measurements are quantitatively consistent with the random component error model to higher wind speeds than are the scatterometer measurements. Along-wind random component error magnitudes for all three satellite datasets were negligibly different (between 0.7 and 1 m/s), while the across-wind random component error magnitudes for WindSat products (2.8 m/s for NESDIS0, 2.6 m/s for B1) were larger than the QuikSCAT value of 2.0 m/s based on buoy comparisons from this time period only. This finding is consistent with the larger direction difference standard deviations for the WindSat–buoy versus QuikSCAT-buoy comparisons.

Global WindSat–QuikSCAT collocations that were constructed and analyzed for the NESDIS0 dataset provided additional insight into the characteristics of the WindSat wind estimates; in particular, the global satellite–satellite comparisons extended both the geographical domain and the range of atmospheric conditions sampled beyond that possible with the NDBC buoys alone. Both the buoy and the satellite–satellite comparisons indicated that the NESDIS0 dataset produced winds with a slightly narrower distribution of speeds near the mean wind speed than any other dataset, and the NESDIS0 directional histogram was distorted, especially near the maximum at directions around 280° (relative to north, oceanographic convention; Figs. 2 and 12). After explicitly accounting for random component errors in both the NESDIS0 and QuikSCAT measurements based on the buoy analyses, the satellite–satellite comparisons generally confirmed the quantitative random component error magnitudes calculated from the buoy analyses (Figs. 9 and 11). At QuikSCAT wind speeds below 4 m/s, the two satellite datasets agreed better than predicted by the component error model. However, the NESDIS0 speeds diverged systematically (NESDIS0 low) from the QuikSCAT measurements for QuikSCAT speeds exceeding $\sim$20 m/s (Fig. 9), in contrast with the (admittedly sparsely sampled) high wind speed buoy comparisons for which the WindSat speeds exceeded the buoy speeds. The global speed comparison results suggest that model function high wind speed refinements may be profitable.

The global comparisons identified a small, but nonnegligible, fraction of collocations for which there were large (>10 m/s) speed differences between spatially and temporally collocated NESDIS0 and QuikSCAT measurements (Fig. 8). For most observed winds (speeds under 20 m/s), these discrepancies corresponded to erroneously high NESDIS0 speed estimates. Although only 0.04% of all measurements had such large discrepancies, these errors—even if randomly distributed in space and time—will significantly distort calculations of key ocean and atmosphere forcing derivative quantities such as surface divergence and wind stress curl, thus detracting from the utility of the WindSat data at high temporal resolution.

Normalized histograms of satellite wind direction as a function of NESDIS0 speed from the collocated global dataset (Fig. 13) provide clues to the causes of the distorted NESDIS0 wind direction histograms. Discontinuities that appear at all directions at NESDIS0 speeds of 4–5 m/s, and discontinuities over speed ranges at directions near 90 and 270° suggest that small refinements may be necessary in the model function or the wind retrieval algorithms.

Rain contamination significantly degrades the accuracy of satellite microwave wind velocity measurements (Figs. 17, 18, 23, and 24). It is thus necessary to identify rain-contaminated data and eliminate it from ground processing (especially ambiguity removal) and subsequent geophysical analysis. However, since important ocean forcing features are often correlated with rain, it is essential to avoid overflagging for rain and thus biasing satellite-based forcing fields more than is necessary (e.g., [35]). This study's comparisons with SSM/I rain measurements in the vicinity of the buoys, as well as comparisons between WindSat and QuikSCAT coverages (Figs. 14) showed that flags based only on relatively simple, direct analyses of WindSat T_b measurements in both the NESDIS0 and the B1 dataset resulted in systematic overflagging for rain, with increasing errors associated with increasing true wind speed (Fig. 19). The improved "EDR" wind flag provided in the B1 dataset clearly decreases the number of cases of overflagging, while preserving the accuracy of the measurements for which the rain flag is not set.

ACKNOWLEDGMENT

WindSat vector wind data were obtained from the Physical Oceanography Distributed Data Archive (PO.DAAC) at the Jet Propulsion Laboratory, Pasadena, CA. SSM/I data are produced by Remote Sensing Systems and sponsored by the NASA Earth Science REASoN DISCOVER Project. Data are available at www.remss.com, and were provided by F. Wentz. Z. Jelenak, M. Bettenhausen, P. Gaiser, D. Long, and F. Monaldo provided helpful comments.

REFERENCES

[1] P. W. Gaiser, K. M. St. Germain, E. M. Twarog, G. A. Poe, W. Purdy, D. Richardsom, W. Grossman, W. L. Jones, D. Spencer, G. Golba, J. Cleveland, L. Choy, R. M. Bevilacqua, and P. S. Chang, "The WindSat spaceborne polarimetric microwave radiometer: Sensor description and early orbit performance," *IEEE Trans. Geosci. Remote Sens.*, vol. 42, no. 11, pp. 2347–2361, Nov. 2004.

[2] W. T. Liu, "Progress in scatterometer applications," *J. Oceanogr.*, vol. 58, pp. 121–136, 2002.

[3] F. M. Naderi, M. H. Freilich, and D. G. Long, "Spaceborne radar measurement of wind velocity over the ocean—An overview of the NSCAT scatterometer system," *Proc. IEEE*, vol. 79, no. 6, pp. 850–856, Jun. 1991.

[4] F. Monaldo, "Expected differences between buoy and radar altimeter estimates of wind speed and significant wave height and their implications on buoy-altimeter comparisons," *J. Geophys. Res.*, vol. 93, pp. 2285–2303, 1988.

[5] D. Offiler, "The calibration of the ERS-1 satellite scatterometer winds," *J. Atmos. Oceanic Technol.*, vol. 11, pp. 1002–1017, 1994.

[6] M. H. Freilich, "Validation of vector magnitude datasets: Effects of random component errors," *J. Atmos. Oceanic Technol.*, vol. 14, pp. 695–703, 1997.

[7] M. H. Freilich and R. S. Dunbar, "The accuracy of the NSCAT 1 vector winds: Comparisons with National Data Buoy Center buoys," *J. Geophys. Res.*, vol. 104, pp. 11 231–11 246, 1999.

[8] W. Tang, W. T. Liu, and B. W. Stiles, "Evaluation of high-resolution ocean surface vector winds measured by QuikSCAT scatterometer in coastal regions," *IEEE Trans. Geosci. Remote Sens.*, vol. 42, no. 8, pp. 1762–1769, Aug. 2004.

[9] A. Stoffelen, "Toward the true near-surface wind speed: Error modeling and calibration using triple collocation," *J. Geophys. Res.*, vol. 103, pp. 7755–7766, 1998.

[10] W. G. Large, J. Morzel, and G. B. Crawford, "Accounting for surface wave distortion of the marine wind profile in low-level Ocean Storms measurements," *J. Phys. Oceanogr.*, pp. 2959–2971, 1995.

[11] D. B. Chelton and M. H. Freilich, "Scatterometer-based assessment of 10-m wind analyses from the operational ECMWF and NCEP numerical weather prediction models," *Mon. Weather Rev.*, vol. 133, pp. 409–429, 2005.

[12] Z. Jelenak, "WindSat polarimetric brightness temperature measurements: Part I—An empirical model," *IEEE Trans. Geosci. Remote Sens.*, 2005, submitted for publication.

[13] ——, "WindSat polarimetric brightness temperature measurements: Part II—Ocean surface wind vector retrievals," *IEEE Trans. Geosci. Remote Sens.*, 2005, submitted for publication.

[14] T. Lungu, "WindSat data products user's manual: Sensor and Environmental Data Records. Version 1.0," Jet Propulsion Lab., Pasadena, CA, Tech. Rep. D-29825, Aug. 2004.

[15] S. H. Yueh, W. J. Wilson, F. K. Li, W. B. Ricketts, and S. V. Nghiem, "Polarimetric brightness temperatures of sea surfaces measured with aircraft K- and Ka-band radiometers," *IEEE Trans. Geosci. Remote Sens.*, vol. 33, no. 5, pp. 1177–1187, Sep. 1997.

[16] S. H. Yueh, W. J. Wilson, S. J. DiNardo, and F. K. Li, "Polarimetric brightness signatures of ocean wind direction," *IEEE Trans. Geosci. Remote Sens.*, vol. 37, no. 2, pp. 949–959, Mar. 1999.

[17] M. H. Bettenhausen, C. K. Smith, R. M. Bevilacqua, N.-Y. Wang, P. W. Gaiser, and S. Cox, "A nonlinear optimization algorithm for WindSat wind vector retrievals," *IEEE Trans. Geosci. Remote Sens.*, vol. 44, no. 3, pp. 597–610, Mar. 2006.

[18] Z. Jelenak, T. Mavor, L. Connor, N.-Y. Wang, P. S. Chang, and P. Gaiser, "Validation of ocean wind vector retrievals from WindSat polarimetric measurements," presented at the *4th Int. Asian-Pacific Environmental Remote Sensing Conf.*, Honolulu, HI, 2004.

[19] T. Lungu, "QuikSCAT science data products user's manual: Overview and geophsyical data products. Version 2.2," Jet Propulsion Lab., Pasadena, CA, Tech. Rep. D-18035, Dec. 2001. [Online]. Available: ftp://podaac.jpl.nasa.gov/pub/ocean_wind/quikscat/doc/QSUG44.pdf.

[20] J. N. Huddleston and B. W. Stiles, "Multidimensional histogram (MUDH) rain flag product description. Version 3.0," Jet Propulsion Lab., Pasadena, CA, Tech. Rep., May 2000. [Online]. Available: ftp://podaac.jpl.nasa.gov/pub/ocean_wind/quikscat/L2B/doc/MUDH_Description_V3.pdf.

[21] B. W. Stiles and S. H. Yueh, "Impact of rain on spaceborne Ku-band wind scatterometer data," *IEEE Trans. Geosci. Remote Sens.*, vol. 40, no. 9, pp. 1973–1983, Sep. 2002.

[22] N. H. Ebuchi, H. C. Graber, and M. J. Caruso, "Evaluation of wind vectors observed by QuikSCAT/SeaWinds using ocean buoy data," *J. Atmos. Oceanic Technol.*, vol. 19, pp. 2049–2062, 2002.

[23] M. A. Portabello and A. Stoffelen, "Characterization of residual information for seawinds quality control," *IEEE Trans. Geosci. Remote Sens.*, vol. 40, no. 12, pp. 2747–2759, Dec. 2002.

[24] D. B. Gilhousen, "A field evaluation of NDBC moored buoy winds," *J. Atmos. Oceanic Technol.*, vol. 4, pp. 94–104, 1987.

[25] R. C. Beardsley, A. G. Enriquez, C. A. Friehe, and C. A. Alessi, "Intercomparison of aircraft and buoy measurements of wind and wind stress during SMILE," *J. Atmos. Oceanic Technol.*, vol. 14, pp. 969–977, 1997.

[26] W. T. Liu and W. Tang, "Equivalent neutral wind," Jet Propulsion Lab., Pasadena, CA, JPL Pub. 96-17, 1996.

[27] D. B. Chelton, M. G. Schlax, M. H. Freilich, and R. F. Milliff, "Satellite measurements reveal short-scale features in the wind stress field over the ocean," *Science*, vol. 303, pp. 978–983, 2004.

[28] R. M. Samelson, P. Barbour, J. Barth, S. Bielli, T. Boyd, D. B. Chelton, P. M. Kosro, M. D. Levine, E. Skyllingstad, and J. M. Wilczak, "Wind stress forcing of the oregon coastal ocean during the 1999 upwelling season," *J. Geophys. Res.*, vol. 107, 2002. DOI: 10.1029/2001JC000900.

[29] T. Shimada and H. Kawamura, "Wind jets and wind waves off the Pacific coast of northern Japan under winter monsoon captured by combined use of scatterometer, synthetic aperture radar, and altimeter," *J. Geophys. Res.*, vol. 109, 2004. DOI: 10.1029/2004JC002450.

[30] B. A. Vanhoff and M. H. Freilich, "Anisotropic random component errors from satellite–satellite scatterometer comparisons," *J. Atmos. Oceanic Technol.*, 2006, submitted for publication.

[31] F. J. Wentz and R. W. Spencer, "SSM/I rain retrievals within a unified all-weather algorithm," *J. Atmos. Sci.*, vol. 55, pp. 1613–1627, 1998.

[32] D. E. Weissman, M. A. Bourassa, and J. Tongue, "Effects of rain rate and wind magnitude on SeaWinds scatterometer wind speed errors," *J. Atmos. Oceanic Technol.*, vol. 19, pp. 738–746, 2002.

[33] D. W. Draper and D. G. Long, "Simultaneous wind and rain retrieval using SeaWinds data," *IEEE Trans. Geosci. Remote Sens.*, vol. 42, no. 7, pp. 1411–1423, Jul. 2004.

[34] ——, “Evaluating the effect of rain on SeaWinds scatterometer measurements,” *J. Geophys. Res.*, vol. 109, 2004. DOI: 10.1029/2002JC001741.

[35] R. F. Milliff, J. Morzel, D. B. Chelton, and M. H. Freilich, “Wind stress curl and divergence biases from rain effects on QuikSCAT surface wind retrievals,” *J. Atmos. Oceanic Technol.*, vol. 21, pp. 1216–1231, 2004.

Michael H. Freilich received B.S. degrees in physics and chemistry from Haverford College, Haverford, PA, in 1975, and the Ph.D. degree in oceanography from Scripps Institution of Oceanography, University of California, San Diego, in 1982, where he studied nonlinear interactions in shoaling waves.

From 1983 through 1991, he was a member of the Technical Staff at the Jet Propulsion Laboratory, California Institute of Technology, where he was NSCAT Project Scientist and the Principal Investigator for the QuikSCAT and SeaWinds scatterometer missions. He joined the faculty of Oregon State University, Corvallis, in 1992, where he is currently Professor and Associate Dean of the College of Oceanic and Atmospheric Sciences.

Dr. Freilich was awarded the AMS Verner E. Suomi Medal “for pioneering the development and scientific application of satellite scatterometery as an essential oceanographic tool” in 2004. He is a Fellow of the American Meteorological Society.

Barry A. Vanhoff received the B.S., M.S., and Ph.D. degrees in electrical engineering from Washington State University, Pullman, in 1988, 1989, and 1996, respectively.

From 1996 to 1998, he studied higher order spectral analysis and nonlinear dynamics as a postdoctoral student at Washington State University. In 1998, he joined the faculty of the College of Oceanic and Atmospheric Sciences, Oregon State University, Corvallis, as a Research Associate, where he is currently developing advanced techniques for satellite vector wind validation and geophysical analyses.